

GENERAL ARTICLE

Imprinting effects of UBE3A loss on synaptic gene networks and Wnt signaling pathways

S. Jesse Lopez^{1,2,3,4,5}, Benjamin I. Laufer^{1,2,5,†}, Ulrika Beitnere^{2,4,5}, Elizabeth L. Berg^{5,6}, Jill L. Silverman^{5,6}, Henriette O'Geen^{2,4,5}, David J. Segal^{2,3,4,5} and Janine M. LaSalle^{1,2,3,5,*}

¹Medical Immunology and Microbiology, University of California (UC) Davis School of Medicine, Davis, CA 95616, USA, ²Genome Center, UC Davis, Davis, CA, USA, ³Integrative Genetics and Genomics, UC Davis, Davis, CA 95616, USA, ⁴Biochemistry and Molecular Medicine, UC Davis School of Medicine, Davis, CA 95616, USA, ⁵Medical Investigation of Neurodevelopmental Disorders Institute, UC Davis Health, Sacramento, CA 95817, USA, and ⁶Psychiatry and Behavioral Sciences, UC Davis School of Medicine, Sacramento, CA 95817, USA

*To whom correspondence should be addressed at: Medical Microbiology and Immunology, One Shields Ave., Davis, CA 95616, USA. Tel: +530 7547598; Fax: +530 7528692; Email: jmlasalle@ucdavis.edu

Abstract

Ubiquitin E3 ligase 3A (UBE3A) encodes an E3 ubiquitin ligase whose loss from the maternal allele causes the neurodevelopmental disorder Angelman syndrome (AS). Previous studies of UBE3A function have not examined full *Ube3a* deletion in mouse, the complexity of imprinted gene networks in brain nor the molecular basis of systems-level cognitive dysfunctions in AS. We therefore utilized a systems biology approach to elucidate how UBE3A loss impacts the early postnatal brain in a novel CRISPR/Cas9-engineered rat Angelman model of a complete *Ube3a* deletion. Strand-specific transcriptome analysis of offspring from maternally or paternally inherited *Ube3a* deletions revealed the expected parental expression patterns of *Ube3a* sense and antisense transcripts by postnatal day 2 (P2) in hypothalamus and day 9 (P9) in cortex, compared to wild-type littermates. The dependency of genome-wide effects on parent-of-origin, *Ube3a* genotype and time (P2 and P9) was investigated through transcriptome (RNA sequencing of cortex and hypothalamus) and methylome (whole-genome bisulfite sequencing of hypothalamus). Weighted gene co-expression and co-methylation network analyses identified co-regulated networks in maternally inherited *Ube3a* deletion offspring enriched in postnatal developmental processes including Wnt signaling, synaptic regulation, neuronal and glial functions, epigenetic regulation, ubiquitin, circadian entrainment and splicing. Furthermore, we showed that loss of the paternal *Ube3a* antisense transcript resulted in both unique and overlapping dysregulated gene pathways with maternal loss, predominantly at the level of differential methylation. Together, these results provide a holistic examination of the molecular impacts of UBE3A loss in brain, supporting the existence of interactive epigenetic networks between maternal and paternal transcripts at the *Ube3a* locus.

†Benjamin I. Laufer, <http://orcid.org/0000-0002-7558-1335>

Received: June 17, 2019. Revised: August 21, 2019. Accepted: September 4, 2019

© The Author(s) 2019. Published by Oxford University Press. All rights reserved. For Permissions, please email: journals.permissions@oup.com

Introduction

Ubiquitin E3 ligase 3A (UBE3A) encodes an E3 ubiquitin ligase that targets multiple proteins for proteasomal degradation (1,2). Residing within the human 15q11.2-q13.3 locus, UBE3A is parentally imprinted, specifically in mature neurons but not glia, where it becomes silenced on the paternal allele due to the paternal-specific expression of an antisense transcript (UBE3A-ATS) originating from an unmethylated imprinting control region on the paternal allele. Angelman syndrome (AS) is a neurogenetic disorder caused by deletion of the maternal 15q11.2-q13.3 locus or maternal-specific UBE3A mutation (3). However, a large population-based study recently demonstrated that both maternal and paternal duplications of 15q11.2-q13.3 are associated with increased risk of autism spectrum disorders or developmental delays (4). Paternal transcripts expressed within human 15q11.2-q13.3 include a long polycistronic transcript encoding the splicing protein SNRPN, snoRNA host genes with independent functions that also produce multiple non-coding snoRNA subunits, as well as UBE3A-ATS. Loss of the paternally expressed SNORD116 locus causes Prader-Willi syndrome (PWS) and results in circadian-dependent changes in gene expression and DNA methylation genome-wide in cortex (5,6), as well as cognitive impairments (7). However, the mechanisms behind how the similarly regulated paternal UBE3A-ATS transcript may contribute to endophenotypes is currently unknown.

Recent research has illuminated diverse roles for UBE3A in neuronal and cellular functions. Proteomic analyses have suggested that UBE3A and its interacting proteins integrate several cellular processes including translation, intracellular trafficking and cytoskeleton regulation, which are all necessary for neuronal function (8,9). In line with its role in neurodevelopmental disease, UBE3A has also been shown to be critical in synaptic formation and maintenance (10–12). We have also recently examined the nuclear chromatin-related genome-wide effects of UBE3A dysregulation in neurons, which revealed significant effects on DNA methylation profiles that were characterized by differentially methylated regions (DMRs) in genes involved in transcriptional regulation and brain development (13). How these diverse functions might contribute to UBE3A-related disorders *in vivo* has yet to be explored.

Over the past decade, rapid progress has been made in understanding biological networks formed by complex sets of interactions between numerous coding and non-coding genes that play important role in deciphering disease phenotypes (14,15). Gene co-expression analysis in particular was designed to identify correlated patterns of gene expression across different experiments, tissues or species (16–19). In particular, gene expression networks have been increasingly used to obtain systematic views about an immensely complex molecular landscape across brain development (20–25). One recent approach for analyzing gene co-expression networks is to identify topological overlap between functional modules or subnetworks that are relevant to the disease. Module discovery using the weighted gene co-expression network analysis (WGCNA) package (17,26) is a widely utilized method for this purpose. WGCNA aims to identify modules of genes that are highly correlated based on their co-expression patterns and does not depend on statistically significant differential expression at the single gene level. The usefulness of this systems biology method has been widely demonstrated as evidenced by multiple publications from a broad range of diseases such as cancer,

epilepsy, neurodegenerative and neurodevelopmental disorder (25,27–29).

To gain stronger insight into how the diverse functions of UBE3A influence neurodevelopment, we leveraged a systems biology approach to examine a novel UBE3A CRISPR-deletion AS rat model and integrated the transcriptome [RNA sequencing (RNA-seq)] and methylome [whole genome bisulfite sequencing (WGBS)]. By identifying the genome-wide changes in the developing brain caused by deletion of *Ube3a*, we uncovered networks and pathways affected by UBE3A at both the transcriptomic and epigenomic levels, including neuronal and synaptic processes and critical cellular pathways. In addition, while the overwhelming majority of reports focus solely on the maternal deletion, we utilized reciprocal breeding, so that both the maternal- and paternal-derived deletions were investigated, revealing genome-wide influences of both maternal *Ube3a* and paternal *Ube3a*-Ats transcripts. Adding to the scope, we examined two brain regions at two developmental time points.

Results

The novel CRISPR/Cas9 knockout rat model contains a complete *Ube3a* deletion that enables allele-specific investigations

While *Ube3a* mutant mice have been extensively used as models of AS (30–34), none of these are complete knockouts of the gene. To produce a more robust model of AS and to better understand the functional consequences of maternal UBE3A loss, an AS rat model was designed to completely delete *Ube3a* by targeting CRISPR/Cas9 nucleases to sites flanking *Ube3a* (*Supplementary Material Fig. S1*).

We devised a breeding strategy to produce both maternally and paternally derived *Ube3a* deletions and harvested hypothalamus and cortex from deletion animals and litter-matched controls at postnatal day 2 (P2) and postnatal day 9 (P9) (*Fig. 1*). These two timepoints were chosen because *Ube3a* was expected to become imprinted within the first week of life, based on prior studies in mouse (35,36), and this was also the time window when deficits in pup ultrasonic vocalization and developmental delays were observed in maternal *Ube3a* deletion rat pups when compared to wild-type littermates (37). RNA-seq browser tracks for hypothalamus and cortex (*Fig. 2*) confirmed the expected loss of the *Ube3a* sense transcript (blue) in maternal *Ube3a* deletion (Mat^{−/−}) samples at both time points when compared to Mat^{+/+} wild-type. In contrast, paternally inherited *Ube3a* deletion (Pat^{−/−}) hypothalamus and cortex samples exhibited the complete loss of the *Ube3a*-Ats transcript (red) when compared to wild-type. In maternally derived *Ube3a* deletion hypothalamic P2 and P9 samples, expression from the *Ube3a* exons is reduced to ~20% of wild-type control, which is consistent with the expected bi-allelic expression in glia. In contrast, expression of *Ube3a*-Ats over the *Ube3a* gene body is almost completely lost in the paternally derived deletion samples, which was expected based on the imprinted expression in all tissues. In the hypothalamus, both *Ube3a* and *Ube3a*-Ats were equivalent at both the P2 and P9 time points (*Supplementary Material Fig. 2*), indicating that *Ube3a* is imprinted prior to P2 in rat hypothalamus, consistent with recent estimates in mouse (38). In cortex, however, both *Ube3a* and *Ube3a*-Ats significantly increased from P2 to P9 (*Supplementary Material Fig. S2*), which is also consistent with findings in mouse of a delayed onset of developmental *Ube3a* imprinting in cortex compared with subcortical brain regions.

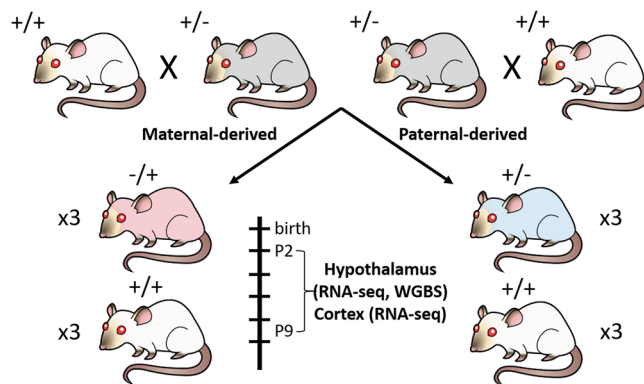


Figure 1. *Ube3a* CRISPR-deletion rat model study design. Reciprocal crosses with *Ube3a*-deletion carriers (gray) produced the maternal-derived (red) and paternal-derived (blue) deletion. Hypothalamus and cortex were harvested from female rat pups at P2 and P9 in triplicate with litter-matched controls and utilized for RNA-seq and WGBS.

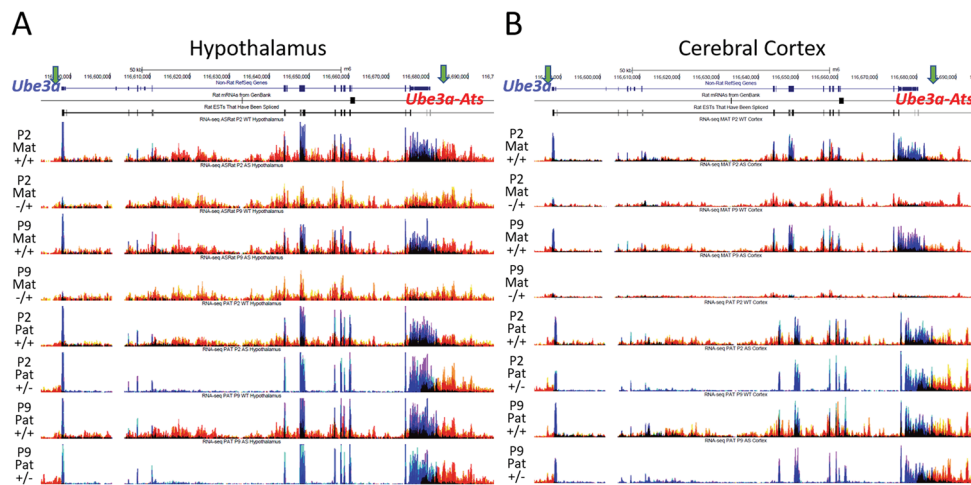


Figure 2. Imprinting patterns of *Ube3a* and *Ube3a*-Ats observed by strand-specific RNA-seq tracks. RNA-seq tracks at the *Ube3a* locus for hypothalamus (left) and cortex (right) samples showing sense-strand (blue) and antisense-strand (red) expression. Maternal deletion samples (P2 Mat -/+ and P9 Mat -/+) displayed a loss of exonic *Ube3a* whereas paternal deletion samples (P2 Pat -/+ and P9 Pat -/+) showed a loss of *Ube3a*-Ats over the deleted *Ube3a* gene body. Quantitation and statistics are provided in [Supplementary Material Table S2](#).

Table 1. WGCNA module summary

Tissue	Deletion parent of origin	Assay	Input genes/regions	Total number of modules	Significant genotype modules (neg:pos)	Genotype genes (neg:pos)	Significant time modules (neg:pos)	Time genes (neg:pos)
Hypothalamus	Maternal	RNA	25 562	26	1:1	149:294	1:2	672:1006
		Methyl	18 335	45	4:4	1587:2028	4:4	1309:1858
	Paternal	RNA	34 812	18	0:0	0:0	2:1	2354:194
		Methyl	13 874	32	2:4	726:1534	4:2	2011:875
	Control	RNA	27 730	18	0:3	0:2774	0:3	0:1361
		Methyl	16 243	0	—	—	—	—
Cortex	Maternal	RNA	34 470	18	1:0	1209:0	5:1	4301:5389
	Paternal	RNA	33 273	38	1:1	150:156	4:3	4725:1009
	Control	RNA	34 318	20	1:0	2271:0	0:0	0:0

Identification of dysregulated gene functions and pathways by *Ube3a* genotype, parental origin and postnatal age from RNA-seq and WGBS

To identify genes dysregulated at the transcript level as a result of *Ube3a* deletion across developmental time, we first performed a standard pairwise differential gene expression

(DGE) analysis using four comparison groups based on time point or parental genotype ([Supplementary Material Figs S3 and S4; Table 1](#)). While *Ube3a* and a few other transcripts reached genome-wide significance for differential expression based on genotype, the complexities in our experimental design to examine genotype parent-of-origin and time interactions were overall not well served by this standard

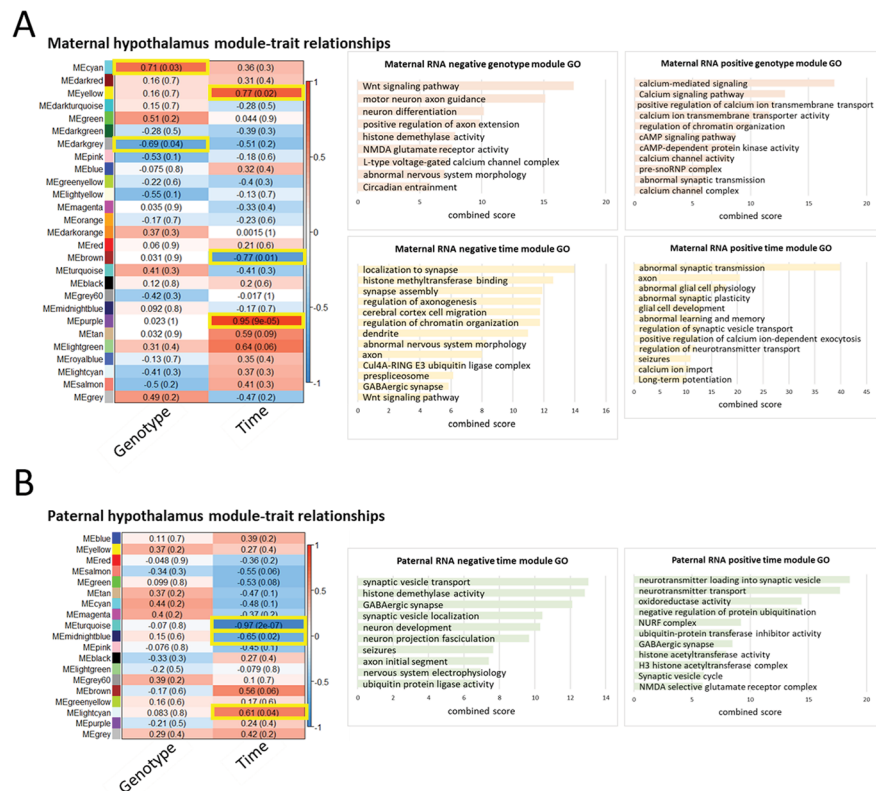


Figure 3. WGCNA expression module and trait correlation heatmaps and GO terms. Co-expression modules detected from network analysis of RPKM in (A) maternal and (B) paternal deletion hypothalamus. Modules were grouped by co-expression and tested for correlation with the traits of genotype or time. Modules of interest are correlated (red) or anti-correlated (blue) with genotype or time (P -value < 0.05 , highlighted yellow boxes). Highlighted co-expression module gene lists were used for GO enrichment with Enrichr using GO Biological Process 2018, GO Cellular Component 2018, GO Molecular Function 2018, KEGG 2016 and MGI Mammalian Phenotype Level 4 categories. Top GO categories are displayed as combined score, calculated as $-\log_{10}(P\text{-value})^z$ -score.

pairwise bioinformatic approach. Similarly, we performed pairwise DMR analyses for either genotype or time using the other as a covariate (Supplementary Material Figs S5–S7; Supplementary Material Table S2), revealing a similarly large number of pairwise DMRs across the entire genome.

Because of the likelihood for interactions of parent-of-origin imprinting effects and postnatal age with *Ube3a* deletion, we sought to improve the analysis of transcriptomic and methylomic data using a systems biology approach. We therefore utilized WGCNA to first identify groups of co-expressed or co-methylated genes and then measure their correlation with either postnatal age or *Ube3a* genotype (sample cluster dendograms in Supplementary Material Fig. S8). We used a litter-based approach where we performed independent WGCNA on data from either the maternal- or paternal-derived litters (weighted network scale-free topology, Supplementary Material Fig. S9). In addition to wild-type littermate controls being included in litter-based WGCNA, control WGCNA were also performed on wild-type offspring across maternal- versus paternal-derived litters as a comparison for background litter effects.

Co-expressed gene modules were detected and tested for correlation with either time point or genotype in separate analyses of hypothalamus (Fig. 3) and cortex (Supplementary Material Fig. S10). Positively correlated modules in red represent increased expression or methylation in *Ube3a* deletion samples compared to wild-type or P9 samples compared to P2. Correlations colored in blue were negative, indicating decreased expression or methylation in *Ube3a* deletion samples or at P9

relative to P2. We then focused on the modules with $P < 0.05$, shown by yellow frames. A summary of the number of WGCNA modules identified and the number passing this significance cutoff is shown in Table 1.

To gain insight into the pathways and networks affected by genotype and time, respectively, these trait-associated modules were used for gene ontology (GO) enrichment. For negatively correlated modules, samples obtained from maternal *Ube3a* deletion and wild-type littermates contained 1 module of 672 co-expressed genes with decreased expression from P2 to P9 in the hypothalamus. Genes within this ‘maternal negative time module’ were enriched in synaptic regulation, epigenetic regulation, axonogenesis, neuron maintenance, ubiquitin activity, splicing and Wnt signaling (Fig. 3A). Two positively correlated maternal time modules containing 1006 genes were enriched in genes with functions in synaptic plasticity and synaptic transmission, glial development and learning and memory. The paternally derived *Ube3a* deletion litters yielded 2 negatively correlated time modules with 2354 genes in hypothalamus and 1 positively correlated module of 194 genes that were similarly enriched in synaptic regulation, epigenetic regulation, neuron development and ubiquitin activity (Fig. 3B). As expected, significant genotype modules were only detected in maternal samples from WGCNA and were enriched in Wnt signaling, neuron differentiation and maintenance, epigenetic regulation, synaptic activity and circadian entrainment for negatively correlated modules, and calcium signaling, chromatin organization and cAMP signaling for positively correlated modules (Fig. 3A). GO enrichment

for negatively correlated modules detected in cortex samples were similar to those observed in hypothalamus modules for time, but the maternal genotype module was distinct in highlighting ubiquitin functions, dendrite and spliceosome in cortex (*Supplementary Material Fig. S11*). A control data set comparing wild-type samples from maternal and paternal litters produced three significant modules for parent-of-origin in hypothalamus and one in cortex with genes enriched in ubiquitin activity (*Supplementary Material Fig. S12*). GO enrichment terms identified by WGCNA were highly similar to those observed by the simpler pairwise analysis (*Supplementary Material Fig. S13*).

For WGCNA of methylation in the hypothalamus, we used the testable ‘background’ regions of potential significant differential methylation from dmrseq to identify gene modules associated with differential methylation by genotype or time (Fig. 4). Co-methylated gene modules were identified similarly to the co-expressed gene modules, focusing on gene modules with the highest confidence correlations for determining GO term enrichments. In contrast to the co-expression analyses in which significant genotype effects were limited to maternal inheritance, multiple co-methylated gene modules based on genotype were observed in both maternal and paternal *Ube3a* deletion litters.

GO analysis of associated genes from co-methylated modules revealed distinctions in gene functions based on maternal versus paternal genotype effects. There were 4 genotype modules with 1366 co-methylated regions detected in maternal samples, which are enriched in neural precursor proliferation, non-canonical Wnt signaling, histone methylation, mTOR, splicing, synaptic activity and ubiquitin activity (Fig. 4A). Whereas, 2 genotype modules with 748 co-methylated regions in paternal samples were identified and were enriched in histone acetylation, excitatory synapse regulation and splicing (Fig. 4B). Time-associated modules were enriched in excitatory synaptic regulation, histone deacetylation, glial differentiation, ubiquitin activity, mTOR and Wnt signaling for maternal samples, while paternal time modules were not only enriched for similar functions but also included imprinting and circadian entrainment. In contrast, the control co-methylation WGCNA from wild-type maternal versus paternal samples not only produced no significant modules but also no clustered modules were detected. Furthermore, GO enrichment terms identified by WGCNA were highly similar to those observed by the pairwise analysis of differentially methylated genes (*Supplementary Material Fig. S13*).

To directly compare the WGCNA results for the co-expression modules and co-methylation modules as well as across parent-of-origin of *Ube3a* deletion, we performed cluster profiling of the GO results for each analysis. For individual GO terms, four distinct clusters were observed for downregulated (negatively correlated modules) specific GO terms (*Supplementary Material Fig. S14*), while the upregulated (positively correlated modules) GO profile clustered into two groups (*Supplementary Material Fig. S15*). Cluster profiling by KEGG pathways revealed five distinct clusters for downregulated pathways (Fig. 5A): Group I clusters by downregulated pathway terms that were specific to maternal, but not paternal, genotype effects, some of which also overlapped with maternal genotype and time-associated co-methylation and paternal time-associated co-methylation terms. These included Wnt signaling, axon guidance and other developmental processes and cancer. Group II clusters by downregulated pathways specific to maternal time-associated co-expression, aside from some associated with paternal time effects. These predominantly included longevity traits as well as insulin, ubiquitin and

choline pathways, which also include genes in RNA metabolic processes. Group III downregulated pathways were uniquely associated with paternal time-associated co-expression, some of which also overlapped with time-associated co-methylation terms. These included GABAergic synapse and genes associated with morphine addiction. Groups IV and V are defined by downregulated pathways uniquely identified by co-methylation, but not co-expression WGCNA. Groups IV and V are distinct in KEGG pathways either largely overlapping by maternal genotype and time (Group IV) or only time-associated but indiscriminate to parental origin (Group V). Group IV included major signal transduction pathways such as MAPK, cAMP, PI3K-Akt and cGMP-PKG, while Group V included pathways related to functions in circadian entrainment, including insulin and oxytocin secretion. KEGG cluster profile for upregulated (positively-correlated) pathways grouped into four patterns (Fig. 5B): Group I clusters the pathways upregulated by maternal *Ube3a* deletion genotype that also overlap with all co-methylation data sets. These pathways are enriched in signaling including calcium, adrenergic and cAMP signaling, as well as serotonergic synapse. Group II clusters the pathways upregulated with time and maternal inheritance that include long-term potentiation, as well as apelin signaling and gastric acid secretion. Groups III and IV cluster pathways commonly upregulated across the co-methylation analyses. Group IV upregulated pathways do not overlap with those identified by maternal genotype and include genes involved in GABAergic and cholinergic synaptic transmission in addition to signaling pathways such as FoxO, Ras and Rap1. Group III clusters the most diverse of the upregulated pathways, which are enriched for the glutamatergic synapse, MAPK signaling, circadian entrainment, Wnt signaling, pluripotency, axon guidance and oxytocin signaling. Paternal time co-expression pathways did not only significantly overlap upregulated pathways but also included GABAergic synapse and synaptic vesicle cycle (*Supplementary Material, Tables S4–S5*). This pathway clustering analysis supports the hypothesis that maternal *Ube3a* genotype effects are predominantly regulating transcriptional differences over time in this AS rat model, while dysregulation in DNA methylation involves contributions of both maternal and paternal *Ube3a* alleles.

Discussion

Together, our data reveals the genome- and epigenome-wide influence of UBE3A on co-regulated genetic networks in a novel rat model with a complete CRISPR/Cas9 knockout of *Ube3a*. We demonstrated that the *Ube3a*-deletion rat model displays the expected transcript levels based on parental imprinting effects in two brain regions. Current AS mouse models contain either a single exon mutation of the maternal *Ube3a* (30), which is not a complete knockout of *Ube3a* similar to the majority of human AS patients, or a large deletion containing part of *Ube3a* extending to *Gabbr3* (39), which confounds the effect of *Ube3a* itself. Moreover, functional AS-relevant phenotypes have been largely dependent on laboratory and background strain of the model (40,41). Given the above considerations, our CRISPR/Cas9 *Ube3a* knockout rat model provides an improved model to study the effects of complete loss of maternal UBE3A as well as the effects of imprinting at this region by reciprocal parental deletions.

Single-gene approaches to analyze the effect of *Ube3a* deletion, such as DGE and DMR analysis, identified specific genes involved in neuronal processes that are affected transcriptionally and epigenetically by loss of both *Ube3a* sense and antisense transcripts. To better understand the co-expression

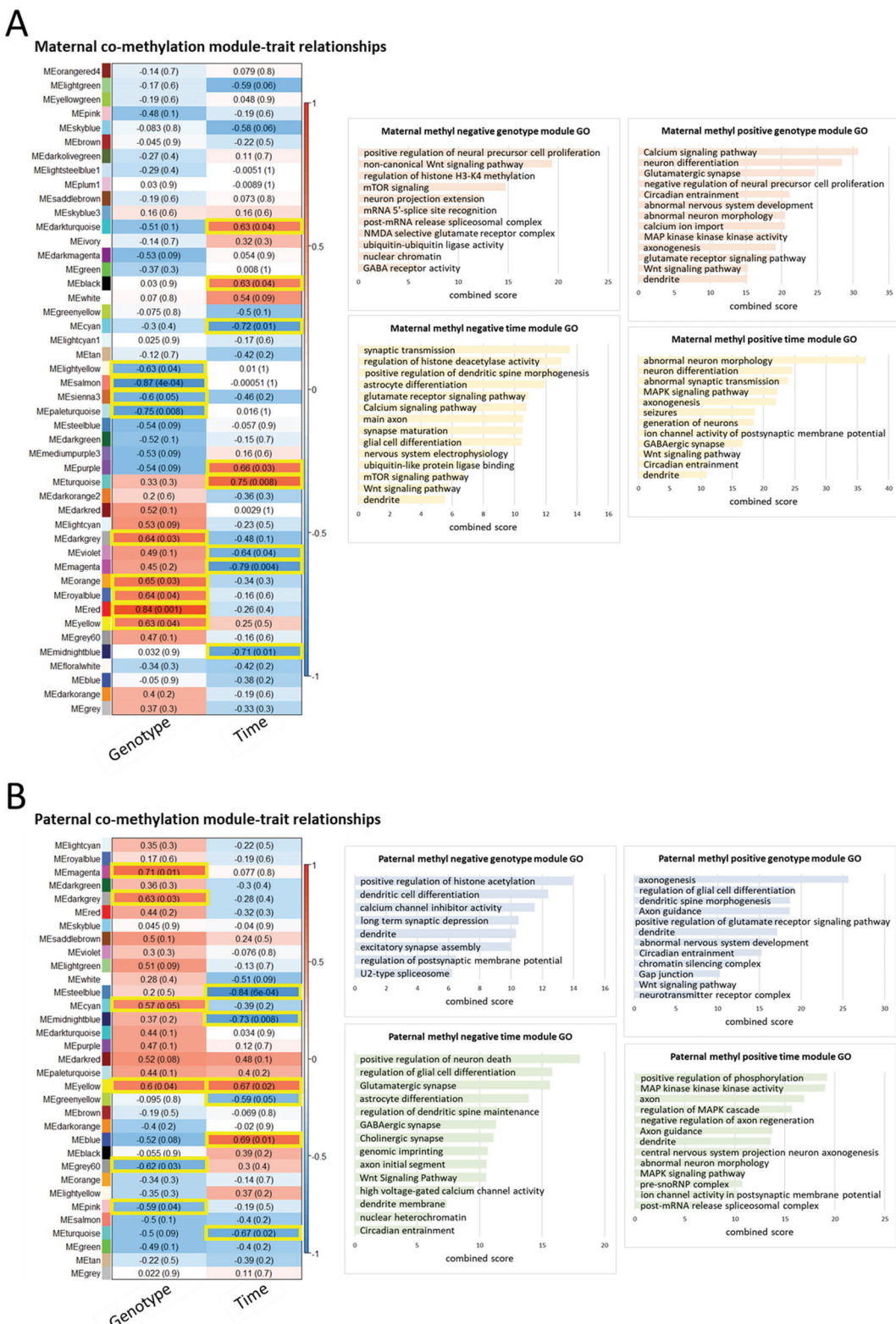


Figure 4. WGCNA methylation module and trait correlation heatmaps and GO terms. Co-methylation modules detected from background smoothed methylation values in maternal and paternal deletion hypothalamus. Modules were grouped by co-expression and tested for correlation with traits of genotype or time. Modules of interest are correlated (red) or anti-correlated (blue) with each trait (P -value < 0.05 , highlighted yellow boxes). Highlighted co-expression module gene lists were used to determine GO enrichment with Enrichr using GO Biological Process 2018, GO Cellular Component 2018, GO Molecular Function 2018, KEGG 2016 and MGI Mammalian Phenotype Level 4 categories. Top GO categories are displayed as combined score, calculated as $-\log_{10}(P\text{-value}) \times z\text{-score}$. Significant module gene lists can be found in Supplementary Material Table S3.

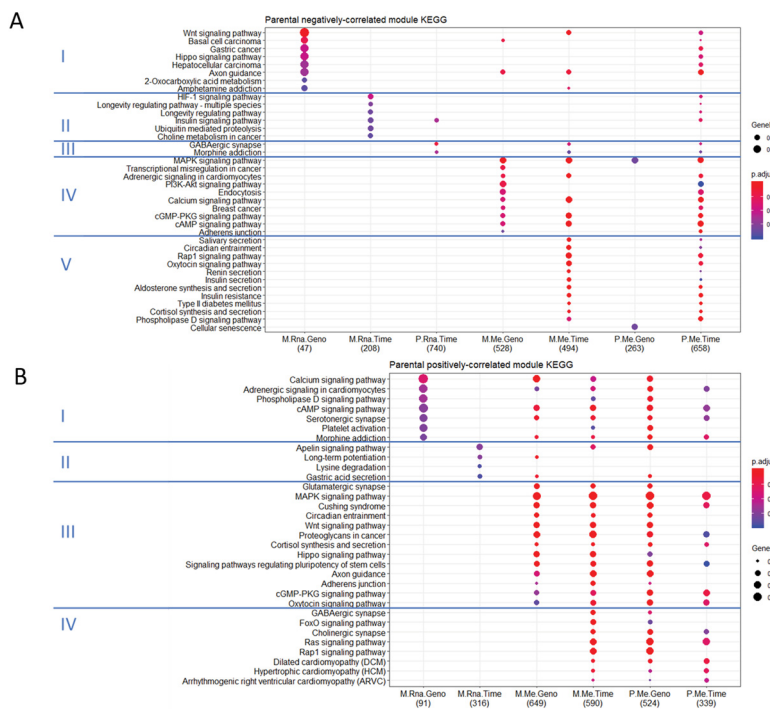


Figure 5. Cluster profiling of functional KEGG pathway enrichments for co-expression and co-methylation analyses. Comparison of KEGG profiles for all data sets using clusterProfiler on (A) negatively correlated and (B) positively correlated modules. Top 10 KEGG enrichment pathways with Benjamini–Hochberg-adjusted *P*-values for each data set are shown. M.Rna.Genotype represents maternal co-expression genotype-significant module genes; M.Rna.Time, maternal co-expression time-significant module genes; P.Rna.Time, paternal co-expression time-significant module genes; M.Me.Genotype, maternal co-methylation genotype-significant module genes; M.Me.Time, maternal co-methylation time-significant module genes; P.Me.Genotype, paternal co-methylation genotype-significant module genes; P.Me.Time, paternal co-methylation time-significant module genes. Full lists of GO terms and associated genes are in Supplementary Material Tables S4 (RNA) and S5 (methylation).

and co-methylation gene network complexities related to *Ube3a*'s parental imprinting and developmental age effects on gene pathways, we also used the systems biology approach of WGCNA. Using WGCNA and associated GO term clustering approaches, we demonstrate that maternal *Ube3a* deletion predominately results in the transcriptional dysregulation of Wnt signaling and other developmental pathways. These results are consistent with the expected maternally inherited phenotypes associated with AS, as well as the brain anatomical differences that were specific to the maternal *Ube3a* deletion offspring in this same AS rat model (37). In this related study, maternal *Ube3a* deletion rats showed significantly smaller cortical regions and significantly larger hypothalamic brain regions, which is consistent with the dysregulated gene pathways involved in developmental and signal transduction pathways observed in our analyses of these two brain regions with maternal *Ube3a* inheritance.

In contrast to the dysregulated gene modules identified by RNA-seq, which were predominantly associated with maternal *Ube3a* deletion, those identified by WGBS methylation analyses were altered mostly equivalently by either maternal or paternal *Ube3a* deletion. These results are consistent with a model in which the maternally expressed protein product UBE3A is upstream of the developmental transcriptional dysregulation in AS, but the non-coding *Ube3a*-Ats regulates reciprocal changes to DNA methylation patterns on both maternal and paternal alleles.

We identified biologically relevant gene networks associated with differential developmental age and genotype in both parentally derived *Ube3a* deletions. Together, these modules shared enrichments for pathways involved in Wnt signaling,

epigenetic regulation, synaptic processes, imprinting, neuro and gliogenesis, circadian entrainment, ubiquitin activity, mTOR and splicing (Fig. 6). Enriched pathways in paternal samples were also seen in the maternal samples including Wnt signaling, ubiquitin, mTOR, neurogenesis, synapse, splicing and epigenetic regulation. Additionally, direct comparison of the functional profiles revealed distinct patterning of network-wide parent-of-origin effects across genotype and developmental time and between the transcriptome and methylome. This approach has revealed that *Ube3a* deletion impacts specific neuronal networks and cellular processes at both the transcriptional and epigenetic level and that the paternally expressed *Ube3a*-Ats transcript has an epigenetic, gene-regulatory function in the developing brain that extends beyond its silencing effect on *Ube3a* sense expression.

Our systems biology approach has identified broad gene networks affected by UBE3A; however, the biological significance of the individual genes identified should be validated by more focused, functional studies. It is also important to note that the relatively small sample size may have limited the power of the network construction in the co-expression analysis compared to the co-methylation networks (scale-free topology; Supplementary Material Fig. S9). How the pathways identified here might inform about the observed behavioral phenotypes will be important to explore in future studies in order to identify novel treatment strategies to ameliorate disease phenotypes. Another limitation of this study is the lack of separation of specific cellular subpopulations of the brain regions. The entirety of the hypothalamus was utilized and a whole hemisphere of cortex was used without sorting of neuron and

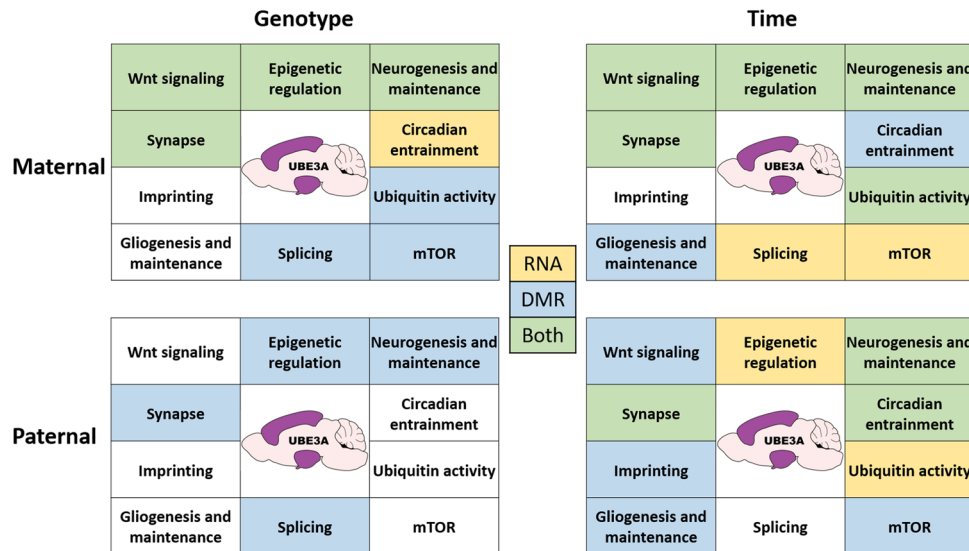


Figure 6. Network enrichment summary. General network categories enriched in WGCNA modules across time and genotype for maternal-derived and paternal-derived deletion samples. Enrichment is denoted for each data set for co-expression modules (yellow), co-methylation modules (blue) or both data sets (green).

glial populations. Since *Ube3a* is not imprinted in glia, the loss of this low level of paternal *Ube3a* expression in glia may have had an impact on our analyses. In future studies, single-cell sequencing approaches to capture expression and methylation differences within distinct cellular subpopulations could provide further insight into the genome-wide impacts of *UBE3A* loss in AS models.

The mechanism by which *Ube3a* is silenced by *Ube3a*-Ats is still not completely understood. *Ube3a*-Ats is at the end of a larger transcript where several additional non-coding RNAs with functions lacking in PWS are processed, particularly the *Snord116* snoRNA and its host gene 116HG (SNHG14). Interestingly, both maternal and paternal *Ube3a* deletion resulted in dysregulated gene pathways that overlapped with those observed with paternal *Snord116* deletion in mouse cortex, including circadian entrainment, mTOR and imprinting (5,6). Together with the results of this study, the evidence suggests that the paternally expressed *Ube3a*-Ats transcript may have similar but non-overlapping functions with SNHG14 and that both maternal and paternal alleles may co-operate in the regulation of circadian rhythms of mTOR-mediated metabolism. These results also fit the recent hypothesized co-evolution of imprinted genes and rapid eye movement sleep patterns in mammals (42,43). Overall, these results suggest a possible cross-talk between maternal and paternal alleles of the AS/PWS loci in regulating DNA methylation changes implicated in the entrainment of circadian rhythmicity in neurons (44).

Materials and Methods

Rat breeding and sample collection

Cas9 and gRNA complexes were injected into fertilized Sprague Dawley rat embryos and inserted into a surrogate. Founders were used to produce F1 progeny, and animals were screened for *UBE3A* expression. Samples were bred in reciprocal crosses from deletion carrier parents to produce maternal- and paternal-derived deletion pups. While no sex differences are observed in AS, we chose to investigate females only to avoid the confounding variable of sex in genomic investigations. Female pups were harvested for tissue at P2 and P9 from 5 litters $n=4$,

2, 4, 1, 1 for maternal samples, and 4 litters $n=3, 3, 4, 2$ for paternal samples. Hypothalamus and cortex were collected and flash frozen, and tail snips were collected for genotyping. Tail snips were prepared using the REDExtract-N-Amp Tissue PCR Kit (Sigma-Aldrich XNAT, St. Louis, MO 63178, USA) and were screened for *Ube3a* deletion using polymerase chain reaction primers spanning the expected deletion site. Brain tissue samples were used for DNA and RNA extraction using the ZR-Duet DNA/RNA MiniPrep Plus Kit (Zymo Genesee 11-385P, Irvine, CA 92614, USA). All procedures were approved by the University of California Davis Institutional Animal Care and Use Committee (IACUC) committee, protocol #20035.

Library preparation and sequencing

RNA from P2 and P9 hypothalamus and cortex was prepared for RNA-seq library using the NEBNext rRNA Depletion Kit (NEB #E6310, Ipswich, MA 01938, USA) and NEBNext Ultra II Directional RNA Library Prep Kit for Illumina (NEB #E7760S, Ipswich, MA 01938, USA). Libraries were assessed for quality control on the Agilent Bioanalyzer 2100. Maternal and paternal libraries were prepared separately then pooled for multiplex sequencing and run 12 samples per lane PE 150 on the HiSeq4000.

DNA from P2 and P9 hypothalamus was used for WGBS. DNA was bisulfite converted using the EZ DNA Methylation-Lightning Kit (Zymo D5031, Irvine, CA, 92614, USA) and prepared for WGBS libraries using the TruSeq DNA Methylation Kit (Illumina EGMK91324, San Diego, CA, 92122, USA). Libraries were assessed for quality control on the Agilent Bioanalyzer 2100. Maternal and paternal samples were prepared separately then pooled for multiplex sequencing and run 12 samples per lane PE 150 on the HiSeqX.

RNA-seq data processing and DGE

Raw fastq files were processed and trimmed using HTStream (<https://github.com/ibest/HTStream>) then used as input for stranded PE alignment using STAR (<https://github.com/alexdobin/STAR>) (45) to output gene count files for each sample. Raw read counts were used for DGE using edgeR (46,47). Briefly, reads

were filtered for one count per million in at least six libraries; libraries were normalized using the weighted trimmed mean of M-values and fit to a single, combined model and extracted pairwise coefficients. DE genes from comparisons were used for GO enrichment analysis using Enrichr (48,49).

WGBS data processing and DMR analysis

Raw fastq files were processed and trimmed of adapters and methylation bias (m-bias) using the CpG_Me repository (https://github.com/ben-laufer/CpG_Me) (50, 51) to generate quality control reports and Bismark cytosine reports for DMR analysis. DMRs and other methylation analyses were performed using the DMRichR package and executable (<https://github.com/ben-laufer/DMRichR>) (50, 52, 53). Briefly, this DMR analysis approach utilizes statistical inference (smoothing) to weight CpG sites based on their coverage. CpGs in physical proximity that also show similar methylation values were then grouped into testable background regions that also showed a difference between groups, and a region statistic for each was estimated. Statistical significance of each testable background region was determined by permutation testing of a pooled null distribution. Annotated DMRs were used for GO enrichment analysis using Enrichr.

Network analysis

Network analysis and module detection were performed using WGCNA (17,26). For co-expression, RPKM was used as input, whereas for co-methylation, background smoothed methylation values output from DMRichR were used. Network construction was done using the blockwiseModules function using maxBlockSize = 5000, minModuleSize = 100 (RNA) or 200 (methylation), TOMType = 'unsigned' (RNA) or 'signed' (methylation) and corType = 'bicor'. Soft-threshold power used in network construction for each data set is shown in Supplementary Material Fig. S9. Significant trait modules determined by Pearson correlation coefficients were subjected to GO enrichment analysis using Enrichr, where co-methylated modules were first annotated using ChIPseeker (54). KEGG enrichment profiling was done using the R package clusterProfiler (55). Ensembl gene ID's for each data set were obtained using rat annotation, and KEGG pathway enrichment was tested using P-value cutoff of 0.1 and Benjamini–Hochberg *q*-value cutoff of 0.5. Top 10 pathways for each group were output.

Data availability

Sequencing data are available in GEO, GSE137217, accession number pending. All the numerical data for the figures and statistics are provided in Supplementary Material.

Supplementary Material

Supplementary Material is available at HMG online.

Author contributions

Data curation and formal analysis by S.J.L. and B.I.L.; conceptualization, supervision and funding acquisition by J.L.S., D.J.S. and J.M.L.; investigation and methodology by S.J.L., B.I.L., U.B., H.O. and E.L.B.; project administration by S.J.L., D.J.S. and J.M.L.; validation, visualization and writing—original draft by S.J.L.; writing—review and editing by B.I.L., J.L.S., D.J.S. and J.M.L.

Funding

National Institutes of Health (R56NS076263 and R01HD098038 to J.M.L. and R01NS097808 to J.L.S.); Intellectual and Developmental Disability Research Center (U54HD079125); Foundation for Angelman Syndrome Therapeutics (J.L.S. and D.J.S.).

Conflict of interest statement

The authors declared they do not have anything to disclose regarding funding or conflict of interest with respect to this manuscript.

References

- Huang, L., Kinnucan, E., Wang, G., Beaudenon, S., Howley, P.M., Huibregtse, J.M. and Pavletich, N.P. (1999) Structure of an E6AP-UbcH7 complex: insights into ubiquitination by the E2–E3 enzyme cascade. *Science*, **286**, 1321–1326.
- Eletr, Z.M. and Kuhlman, B. (2007) Sequence determinants of E2–E6AP binding affinity and specificity. *J. Mol. Biol.*, **369**, 419–428.
- LaSalle, J.M., Reiter, L.T. and Chamberlain, S.J. (2015) Epigenetic regulation of UBE3A and roles in human neurodevelopmental disorders. *Epigenomics*, **7**, 1213–1228.
- Isles, A.R., Ingason, A., Lowther, C., Walters, J., Gawlick, M., Stöber, G., Rees, E., Martin, J., Little, R.B. and Potter, H. (2016) Parental origin of interstitial duplications at 15q11.2-q13.3 in schizophrenia and neurodevelopmental disorders. *PLoS Genet.*, **12**, e1005993.
- Powell, W.T., Crary, F.K., Coulson, R.L., Wong, S.S., Yasui, D.H., LaSalle, J.M., Alice Yamada, N., Tsang, P. and Ach, R.A. (2013) A Prader–Willi locus lncRNA cloud modulates diurnal genes and energy expenditure. *Hum. Mol. Genet.*, **22**, 4318–4328.
- Coulson, R.L., Yasui, D.H., Dunaway, K.W., Laufer, B.I., Vogel Ciernia, A., Zhu, Y., Mordaunt, C.E., Totah, T.S. and LaSalle, J.M. (2018) Snord116-dependent diurnal rhythm of DNA methylation in mouse cortex. *Nat. Commun.*, **9**, 1616.
- Adhikari, A., Copping, N.A., Onaga, B., Pride, M.C., Coulson, R.L., Yang, M., Yasui, D.H., LaSalle, J.M. and Silverman, J.L. (2018) Cognitive deficits in the Snord116 deletion mouse model for Prader–Willi syndrome. *Neurobiol. Learn. Mem.*, in press.
- Martínez-Noël, G., Galligan, J.T., Sowa, M.E., Arndt, V., Overton, T.M., Harper, J.W. and Howley, P.M. (2012) Identification and proteomic analysis of distinct UBE3A/E6AP protein complexes. *Mol. Cell. Biol.*, **32**, 3095–3106.
- Martínez-Noël, G., Luck, K., Kühnle, S., Desbuleux, A., Szajner, P., Galligan, J.T., Rodriguez, D., Zheng, L., Boyland, K., Leclerc, F. et al. (2018) Network analysis of UBE3A/E6AP-associated proteins provides connections to several distinct cellular processes. *J. Mol. Biol.*, **430**, 1024–1050.
- Sun, J., Zhu, G., Liu, Y., Standley, S., Ji, A., Tunuguntla, R., Wang, Y., Claus, C., Luo, Y., Baudry, M. et al. (2015) UBE3A regulates synaptic plasticity and learning and memory by controlling SK2 channel endocytosis. *Cell Rep.*, **12**, 449–461.
- Kim, H., Kunz, P.A., Mooney, R., Philpot, B.D. and Smith, S.L. (2016) Maternal loss of Ube3a impairs experience-driven dendritic spine maintenance in the developing visual cortex. *J. Neurosci.*, **36**, 4888–4894.
- Xu, X., Li, C., Gao, X., Xia, K., Guo, H., Li, Y., Hao, Z., Zhang, L., Gao, D. and Xu, C. (2018) Excessive UBE3A dosage impairs retinoic acid signaling and synaptic plasticity in autism spectrum disorders. *Cell Res.*, **28**, 48.

13. Lopez, S.J., Dunaway, K., Islam, M.S., Mordaunt, C., Vogel Ciernia, A., Meguro-Horiike, M., Horiike, S., Segal, D.J. and LaSalle, J.M. (2017) UBE3A-mediated regulation of imprinted genes and epigenome-wide marks in human neurons. *Epigenetics*, **12**, 982–990.
14. Goh, K.-I., Cusick, M.E., Valle, D., Childs, B., Vidal, M. and Barabási, A.-L. (2007) The human disease network. *Proc. Natl. Acad. Sci. USA*, **104**, 8685–8690.
15. Vidal, M., Cusick, M.E. and Barabási, A.-L. (2011) Interactome networks and human disease. *Cell*, **144**, 986–998.
16. Stuart, J.M., Segal, E., Koller, D. and Kim, S.K. (2003) A gene-coexpression network for global discovery of conserved genetic modules. *Science*, **302**, 249–255.
17. Zhang, B. and Horvath, S. (2005) A general framework for weighted gene co-expression network analysis. *Stat. Appl. Genet. Mol. Biol.*, **4**, 1–4.
18. Henegar, C., Tordjman, J., Achard, V., Lacasa, D., Cremer, I., Guerre-Millo, M., Poitou, C., Basdevant, A., Stich, V., Viguerie, N. et al. (2008) Adipose tissue transcriptomic signature highlights the pathological relevance of extracellular matrix in human obesity. *Genome Biol.*, **9**, R14–R14.
19. Henegar, C., Prifti, E., Zucker, J.-D. and Clément, K. (2010) Interactional and functional centrality in transcriptional co-expression networks. *Bioinformatics*, **26**, 3083–3089.
20. Kang, H.J., Kawasawa, Y.I., Cheng, F., Zhu, Y., Xu, X., Li, M., Sousa, A.M.M., Pletikos, M., Meyer, K.A. and Sedmak, G. (2011) Spatio-temporal transcriptome of the human brain. *Nature*, **478**, 483–489.
21. Willsey, A.J., Sanders, S.J., Li, M., Dong, S., Tebbenkamp, A.T., Muhle, R.A., Reilly, S.K., Lin, L., Fertuzinhos, S. and Miller, J.A. (2013) Coexpression networks implicate human midfetal deep cortical projection neurons in the pathogenesis of autism. *Cell*, **155**, 997–1007.
22. Parikshak, N.N., Luo, R., Zhang, A., Won, H., Lowe, J.K., Chandran, V., Horvath, S. and Geschwind, D.H. (2013) Integrative functional genomic analyses implicate specific molecular pathways and circuits in autism. *Cell*, **155**, 1008–1021.
23. Gulsuner, S., Walsh, T., Watts, A.C., Lee, M.K., Thornton, A.M., Casadei, S., Rippey, C., Shahin, H., Braff, D. and Cadenhead, K.S. (2013) Spatial and temporal mapping of de novo mutations in schizophrenia to a fetal prefrontal cortical network. *Cell*, **154**, 518–529.
24. Lin, G.N., Corominas, R., Lemmens, I., Yang, X., Tavernier, J., Hill, D.E., Vidal, M., Sebat, J. and Iakoucheva, L.M. (2015) Spatiotemporal 16p11.2 protein network implicates cortical late mid-fetal brain development and KCTD13–Cul3–RhoA pathway in psychiatric diseases. *Neuron*, **85**, 742–754.
25. Voineagu, I., Wang, X., Johnston, P., Lowe, J.K., Tian, Y., Horvath, S., Mill, J., Cantor, R.M., Blencowe, B.J. and Geschwind, D.H. (2011) Transcriptomic analysis of autistic brain reveals convergent molecular pathology. *Nature*, **474**, 380–384.
26. Langfelder, P. and Horvath, S. (2008) WGCNA: an R package for weighted correlation network analysis. *BMC Bioinformatics*, **9**, 559.
27. Horvath, S., Zhang, B., Carlson, M., Lu, K.V., Zhu, S., Felciano, R.M., Laurance, M.F., Zhao, W., Qi, S. and Chen, Z. (2006) Analysis of oncogenic signaling networks in glioblastoma identifies ASPM as a molecular target. *Proc. Natl. Acad. Sci. USA*, **103**, 17402–17407.
28. Presson, A.P., Yoon, N.K., Bagryanova, L., Mah, V., Alavi, M., Maresh, E.L., Rajasekaran, A.K., Goodlick, L., Chia, D. and Horvath, S. (2011) Protein expression based multimarker analysis of breast cancer samples. *BMC Cancer*, **11**, 230.
29. Levine, A.J., Miller, J.A., Shapshak, P., Gelman, B., Singer, E.J., Hinkin, C.H., Commins, D., Morgello, S., Grant, I. and Horvath, S. (2013) Systems analysis of human brain gene expression: mechanisms for HIV-associated neurocognitive impairment and common pathways with Alzheimer's disease. *BMC Med. Genomics*, **6**, 4.
30. Jiang, Y., Armstrong, D., Albrecht, U., Atkins, C.M., Noebels, J.L., Eichele, G., Sweatt, J.D. and Beaudet, A.L. (1998) Mutation of the Angelman ubiquitin ligase in mice causes increased cytoplasmic p53 and deficits of contextual learning and long-term potentiation. *Neuron*, **21**, 799–811.
31. Dindot, S.V., Antalffy, B.A., Bhattacharjee, M.B. and Beaudet, A.L. (2008) The Angelman syndrome ubiquitin ligase localizes to the synapse and nucleus, and maternal deficiency results in abnormal dendritic spine morphology. *Hum. Mol. Genet.*, **17**, 111–118.
32. Miura, K., Kishino, T., Li, E., Webber, H., Dikkes, P., Holmes, G.L. and Wagstaff, J. (2002) Neurobehavioral and electroencephalographic abnormalities in Ube3aMaternal-deficient mice. *Neurobiol. Dis.*, **9**, 149–159.
33. Albrecht, U., Sutcliffe, J.S., Cattanach, B.M., Beechey, C.V., Armstrong, D., Eichele, G. and Beaudet, A.L. (1997) Imprinted expression of the murine Angelman syndrome gene, Ube3a, in hippocampal and Purkinje neurons. *Nat. Genet.*, **17**, 75–78.
34. Heck, D.H., Zhao, Y., Roy, S., LeDoux, M.S. and Reiter, L.T. (2008) Analysis of cerebellar function in Ube3a-deficient mice reveals novel genotype-specific behaviors. *Hum. Mol. Genet.*, **17**, 2181–2189.
35. Masuzaki, H., Wagstaff, J., Joh, K., Yamasaki, K., Ogawa, M., Niikawa, N., Ishimaru, T., Kishino, T., Mukai, T. and Ohta, T. (2003) Neurons but not glial cells show reciprocal imprinting of sense and antisense transcripts of Ube3a. *Hum. Mol. Genet.*, **12**, 837–847.
36. Judson, M.C., Sosa-Pagan, J.O., Del Cid, W.A., Han, J.E. and Philpot, B.D. (2014) Allelic specificity of Ube3a expression in the mouse brain during postnatal development. *J. Comp. Neurol.*, **522**, 1874–1896.
37. Berg, E.L., Pride, M.C., Lee, R.D., Coping, N.A., Noakes, L.S., Nieman, B.J., Ellegood, J., Lerch, J.P., Harris, S., Born, H.A. et al. (2018) Developmental social communication in the Ube3a rat model of Angelman syndrome. In Society for Neuroscience, San Diego, CA, p. 119.15/D40.
38. Grier, M.D., Carson, R.P. and Lagrange, A.H. (2015) Toward a broader view of Ube3a in a mouse model of Angelman syndrome: expression in brain, spinal cord, sciatic nerve, glial cells. *PLoS One*, **10**, 1–14.
39. Jiang, Y., Pan, Y., Zhu, L., Landa, L., Yoo, J., Spencer, C., Lorenzo, I., Brilliant, M., Noebels, J. and Beaudet, A.L. (2010) Altered ultrasonic vocalization and impaired learning and memory in Angelman syndrome mouse model with a large maternal deletion from Ube3a to Gabrb 3. *PLoS One*, **5**, e12278.
40. Born, H.A., Dao, A.T., Levine, A.T., Lee, W.L., Mehta, N.M., Mehra, S., Weeber, E.J. and Anderson, A.E. (2017) Strain-dependence of the Angelman syndrome phenotypes in Ube3a maternal deficiency mice. *Sci. Rep.*, **7**, 1–15.
41. Huang, H.-S., Burns, A.J., Nonneman, R.J., Baker, L.K., Riddick, N.V., Nikolova, V.D., Riday, T.T., Yashiro, K., Philpot, B.D. and Moy, S.S. (2013) Behavioral deficits in an Angelman syndrome model: effects of genetic background and age. *Behav. Brain Res.*, **243**, 79–90.
42. Tucci, V. (2016) Genomic imprinting: a new epigenetic perspective of sleep regulation. *PLoS Genet.*, **12**, e1006004.
43. Tucci, V., Isles, A.R., Kelsey, G., Ferguson-Smith, A.C., Bartolomei, M.S., Benvenisty, N., Bourc'his, D., Charalam-

- bous, M., Dulac, C. and Feil, R. (2019) Genomic imprinting and physiological processes in mammals. *Cell*, **176**, 952–965.
44. Azzi, A., Dallmann, R., Casserly, A., Rehrauer, H., Patrignani, A., Maier, B., Kramer, A. and Brown, S.A. (2014) Circadian behavior is light-reprogrammed by plastic DNA methylation. *Nat. Neurosci.*, **17**, 377.
45. Dobin, A., Davis, C.A., Schlesinger, F., Drenkow, J., Zaleski, C., Jha, S., Batut, P., Chaisson, M. and Gingeras, T.R. (2013) STAR: ultrafast universal RNA-seq aligner. *Bioinformatics*, **29**, 15–21.
46. Robinson, M.D., McCarthy, D.J. and Smyth, G.K. (2010) edgeR: a bioconductor package for differential expression analysis of digital gene expression data. *Bioinformatics*, **26**, 139–140.
47. McCarthy, D.J., Chen, Y. and Smyth, G.K. (2012) Differential expression analysis of multifactor RNA-Seq experiments with respect to biological variation. *Nucleic Acids Res.*, **40**, 4288–4297.
48. Chen, E.Y., Tan, C.M., Kou, Y., Duan, Q., Wang, Z., Meirelles, G.V., Clark, N.R. and Ma'ayan, A. (2013) Enrichr: interactive and collaborative HTML5 gene list enrichment analysis tool. *BMC Bioinformatics*, **14**, 128.
49. Kuleshov, M.V., Jones, M.R., Rouillard, A.D., Fernandez, N.F., Duan, Q., Wang, Z., Koplev, S., Jenkins, S.L., Jagodnik, K.M., Lachmann, A. et al. (2016) Enrichr: a comprehensive gene set enrichment analysis web server 2016 update. *Nucleic Acids Res.*, **44**, W90–W97.
50. Laufer, B.I., Hwang, H., Ciernia, A.V., Mordaunt, C.E. and LaSalle, J.M. (2018) Whole genome bisulfite sequencing of Down syndrome brain reveals regional DNA hypermethylation and novel disease insights. *Epigenetics*, **14**, 672–684.
51. Krueger, F. and Andrews, S.R. (2011) Bismark: a flexible aligner and methylation caller for Bisulfite-Seq applications. *Bioinformatics*, **27**, 1571–1572.
52. Korthauer, K., Chakraborty, S., Benjamini, Y. and Irizarry, R.A. (2017) Detection and accurate false discovery rate control of differentially methylated regions from whole genome bisulfite sequencing. *Biostatistics*, **20**, 367–383.
53. Hansen, K.D., Langmead, B. and Irizarry, R.A. (2012) BSmooth: from whole genome bisulfite sequencing reads to differentially methylated regions. *Genome Biol.*, **13**, R83.
54. He, Q.-Y., Yu, G. and Wang, L.-G. (2015) ChIPseeker: an R/bioconductor package for ChIP peak annotation, comparison and visualization. *Bioinformatics*, **31**, 2382–2383.
55. Yu, G., Wang, L.-G., Han, Y. and He, Q.-Y. (2012) clusterProfiler: an R package for comparing biological themes among gene clusters. *OMICS*, **16**, 284–287.